Icarus 385 (2022) 115111

Contents lists available at ScienceDirect

Icarus

journal homepage: www.elsevier.com/locate/icarus

Raman spectroscopic documentation of Mars analog basalt alteration by brines

Andrew Rodriguez [a,*], Lindsey Hunt [a], Charity Phillips-Lander [b], Daniel Mason [c], Megan Elwood Madden [a]

[a] OU School of Geosciences, United States of America
[b] Southwest Research Institute, United States of America
[c] UNM School of Earth and Planetary Sciences, United States of America

ARTICLE INFO

Keywords:
Mars
Brine
Raman spectroscopy
Secondary minerals
Basalt

ABSTRACT

Salts and basalt are widespread on the surface of Mars. Therefore, basalt-brine interactions may have significant effects on both the aqueous history of the planet, and near-surface alteration assemblages. Raman spectra were collected from McKinney Basalt samples that were immersed in eight near-saturated brines composed of Na-Cl-H_2O, Na-SO_4-H_2O, Na-ClO_4-H_2O, Mg-Cl-H_2O, Mg-SO_4-H_2O, and two salt mixtures (Mg-Cl-SO_4-H_2O and Na-ClO_4-SO_4-H_2O), as well as ultra-pure water for up to one year. Secondary minerals were observed in the Raman specta, including iron oxides, hydrated sulfates, amorphous silica, phosphates, and carbonates. Detection of these secondary minerals demonstrates the utility of Raman spectroscopy to identify basalt-brine alteration assemblages on Mars. This work also demonstrates that major classes of alteration phases can be distinguished using Raman spectra with resolution similar to those expected from the Raman instruments aboard the Perseverance and Rosalind Franklin Mars rovers. In addition, observations of carbonate minerals within alteration assemblages suggest CO_2 from the atmosphere readily reacted with ions released from the basalt during alteration in near-saturated brines.

1. Introduction

As we continue to send rovers, landers, and orbiters to Mars, our understanding of the past geologic landscape has broadened to include water-salt interactions in addition to more traditional aspects of an active hydrologic cycle. Geomorphic and geochemical observations, combined with modern atmospheric water vapor fluctuations suggest hydrologic activity may have continued intermittently throughout Mars history (Beck et al., 2020; Bhattacharya et al., 2005; Gaillard et al., 2013; Nachon et al., 2014; Nuding et al., 2014; Ojha et al., 2015; Rennó et al., 2009; Schon et al., 2012). For example, recurring slope lineae (RSL) observed in orbital images may be evidence of upwelling of salty groundwater, or may form from water vapor as a result of the salts present (Abotalib and Heggy, 2019; McEwen et al., 2014), albeit over limited latitudes and time periods (Rivera-Valentín et al., 2020). Droplet-like growths on the Phoenix lander struts as well as images of possible liquid-induced recurring slope lineae at Richardson Crater provide further evidence of modern brines on the surface of Mars (Kieffer, 2007; Martínez et al., 2012). While pure liquid water is not thermodynamically stable under Mars surface conditions and will evaporate rapidly, ubiquitous salts observed by rovers, landers, and orbiters could mix with water to form brines more stable in liquid state than pure or dilute solutions on the Martian surface (Chevrier et al., 2020, 2009; Chevrier and Morisson, 2021; Martín-Torres et al., 2015; Rivera-Valentín et al., 2020). Because dissolved ions lower the freezing point of water, liquid water could be present over at locations on Mars including Gale Crater, Gusev Crater, and Meridiani Planum (Clark and Baird, 1979; Cull et al., 2010; Haberle et al., 2001; Kounaves et al., 2010; Rennó et al., 2009).

Therefore, understanding the role of brines in past– and possibly current– aqueous processes on Mars is necessary for interpreting the geological history of the planet and its potential habitability (Baker et al., 1991; Benison et al., 2008; Bish et al., 2003; Carter et al., 2013; Clark and Baird, 1979; Clifford and Parker, 2001; Goudge et al., 2016; Haskin et al., 2005; Kite, 2019; Rummel et al., 2014; Solomon et al., 2005). Given the abundance of salts and the low temperature and

* Corresponding author.
E-mail address: andrew.rodriguez@ou.edu (A. Rodriguez).

https://doi.org/10.1016/j.icarus.2022.115111
Received 30 January 2021; Received in revised form 23 May 2022; Accepted 24 May 2022
Available online 27 May 2022

pressure conditions, any liquid water present at the surface today is likely very salty, since near-saturated brines are stable over the broadest range of temperature and pressure conditions and timeframes (Carr, 1979; Chevrier et al., 2020; Chevrier and Rivera-Valentin, 2012; Martínez and Renno, 2013; Primm et al., 2017; Temel et al., 2021; Tosca and McLennan, 2009). Furthermore, if high salinity brines have been present on the surface of Mars, they likely interacted with basalts and basalt-sourced sediments common on the surface.

Previous studies have shown that high salinity Na-Cl-H_2O and Na-SO_4-H_2O brines have significant effects on diopside dissolution, despite low water activity (Phillips-Lander et al., 2019). Other studies have also demonstrated that increasing concentrations of Na^+ and Cl^- ions can also increase silicate dissolution rates (Dove et al., 2005). However, it is unclear if such alteration could be observed with current analytical techniques available on Mars. Here we investigate the effectiveness of Raman spectroscopy in detecting and characterizing short-term basalt-brine interactions and their implications for the Mars 2020 and ExoMars missions. In this study we examine basalt dissolution, alteration, secondary mineral precipitation, and possible changes to solution chemistry.

The inclusion of Raman spectrometers on both the Mars 2020 and ExoMars rover missions provides a new opportunity for identifying and analyzing chemical weathering products in situ (Beegle et al., 2015; Rull et al., 2017; Vago et al., 2017). The SuperCam instrument on the Mars 2020 rover uses a 532 nm green laser to study the mineralogy of the Martian surface, and the Scanning Habitable Environments with Raman & Luminescence for Organics & Chemicals instrument (SHERLOC) uses both a 548.6 nm green laser and a 248.6 nm deep ultraviolet (DUV) laser to characterize possible suspect organic molecules (Beegle et al., 2015; Wiens et al., 2017).

Raman spectroscopy is a vibrational spectroscopy technique that can be used to identify covalently bonded materials without the need to prepare or disturb the sample. This allows researchers to discern mineral phases that may occur as a result of aqueous alteration, as different minerals will produce a different Raman spectra due to the unique intramolecular forces in covalently bonded materials (Chou and Wang, 2017; Nikolakakos and Whiteway, 2018). Raman spectrometers can be used to identify minerals based on the inelastic scattering of energy from phonons within a target, and have the potential to distinguish minerals that are similar in chemical composition (Das and Hendry, 2011). In addition, Raman spectroscopic analyses do not require a radioactive source, in contrast to other methods such as alpha particle x-ray spectrometry (APXS)

However, few studies have used Raman spectroscopy as a tool to look for evidence of aqueous weathering in igneous rocks (Bakker, 2004; Frezzotti et al., 2012; Martinez et al., 2004; Wang et al., 2006). In this study we tested the utility of Raman spectroscopy to discern weathering products produced by reacting Mars-analog basalt with near-saturated brines for up to one year. In these moderate-term experiments, brines reacted with the basalt samples and precipitated secondary minerals at a scale which can be discerned with a Raman spectrometer. We used a 532 nm laser similar to the excitation sources used by the SuperCam Raman/LIBS system on NASA's Mars 2020 rover, as well as the RLS Raman Spectrometer on the European Space Agency's ExoMars 2020 rover. Through these experiments and subsequent Raman analyses, we demonstrate that moderate-term basalt-brine weathering products can be observed.

2. Methods

In order to investigate basalt-brine interactions, we placed nine samples of McKinney Basalt (0.1 g to 0.2 g ±0.05 g) in 250 mL wide-mouth round HDPE bottles containing 100 mL of single salt saturated brines (NaCl, Na-SO_4H_2O, Na-ClO_4-H_2O, Mg-SO_4-H_2O, Mg-Cl-H_2O, or Ca-Cl-H_2O), 100 mL of ultra-pure water, or 100 mL of a mixed brine solution (Mg-Cl-SO_4-H_2O, Na-ClO_4-SO_4-H_2O) and analyzed the solid and liquid components to document changes to these components of the samples as time progressed after 3, 6, or 12 months of reaction. These salts were chosen because they have been previously observed on Mars (Brass, 1980; Carrier and Kounaves, 2015; Hanley et al., 2013; Martínez and Renno, 2013; Martín-Torres et al., 2015; Wang et al., 2006). We used McKinney basalt because it has similar bulk chemistry to multiple locations on Mars and Mars meteorites (Adcock et al., 2018; Leeman, 1982; Leeman and Vitaliano, 1976).

The basalt pieces were sonicated to remove fine dust and microscopic grains, then air dried. A subset of fourteen sample chips were cut and hand polished with lapping film to form a single planar surface on each chip for electron microbeam analyses. The chips were further polished with 0.3 μm and 0.05 μm Al_2O_3 powder. These polished chips are referred to as "polished" henceforth to distinguish them from the rough, unpolished samples. For each brine experiment, one polished chip and 11 rough chips were selected and rinsed with 18.2 MΩ H_2O before the experiment.

The brines were produced by adding laboratory grade salts to ultra-pure water in non-reactive plastic containers and constantly agitating the reactors until no further salts dissolved. 100 mL of single-salt saturated brine (Na-Cl-H_2O, Na-SO_4-H_2O, Na-ClO_4-H_2O, Mg-SO_4-H_2O, Mg-Cl-H_2O, Ca-Cl-H_2O) or 100 mL of ultra-pure water (UPW, 18MΩ conductivity) were then placed in separate Nalgene bottle reactors. Two additional reactors contained mixed brines—one with a mixture of 50 mL of Na-ClO_4-H_2O saturated brine and 50 mL of Na-SO_4-H_2O saturated brine, and the other with a mixture of 50 mL of Mg-SO_4-H_2O saturated brine and 50 mL of Mg-Cl-H_2O saturated brine.

Five mL of each solution were extracted before the experiment and used as a control; pH was measured using an Orion 3 Star pH benchtop electrode, with a range from −2.00 to 19.99 ± 0.002. While this probe is designed for general lab use and does not produce highly accurate pH measurements in highly saline solutions, measurements can be used to compare relative pH between solutions and monitor pH change over time. An additional 4 mL of each brine was reserved for Raman analysis, then 0.3 mL sub-samples of each brine were placed into wells on a porcelain painter's dish for analysis with a Renishaw InVia Raman spectrometer using a 532 nm green laser set to streamline laser settings, centered at 1500 wavenumbers (cm^{-1}) with a 1200 lines/cm grating. This provides a wide enough range to include peaks from the polyatomic ions in the brine, the water peak at 1640 wavenumbers, possible secondary minerals in suspension, and/or any new polyatomic ions from chemical reactions. The painter's dish produces no additional peaks in the Raman analysis, allowing for a clear Raman signal from the brines.

Once we collected the control brine samples, we added the basalt chips to each of the nine reactors. The bottles were capped to prevent spills, but we expected atmospheric O_2 and CO_2 to be in equilibrium with the gas inside the bottles since the experiment occurred on a lab bench outside of a controlled environment, we opened the bottles multiple times, and the caps were not a perfect seal. We remeasured the pH of each solution within the first hour of reaction, and then placed the nine bottles, each containing a different experimental solution and 12 basalt chips on a shaker table set for 240 rpm; temperature was maintained at ~25 °C.

After 30 days of we reaction, we removed three rough basalt chips from each reactor and rinsed with 30 mL of ultrapure water or less to remove any brine remaining on the basalt sample surfaces, thus allowing analysis of less soluble secondary phases without obstruction from salt crusts which would form as the brines evaporate. Each rock chip was weighed and placed in a sealed plastic bag with a dry paper towel for storage. We extracted 7 mL from the 100 mL of solution, with 3 mL used for pH measurements and 4 mL used for Raman spectroscopy. The reactors were then recapped and returned to the shaker table to continue agitation.

Within 24 h of sampling, Raman spectra were collected from the reacted basalt samples using the 532 nm laser with a 1200 l/cm grating centered at 1500 cm^{-1}. The laser was focused on a one micron diameter

spot on the surface of each basalt sample at 10% power for 240 s each. Raman spectra were collected at different locations on the basalt sample until at least three separate spectra were collected that were indicative of each of the primary minerals observed in the McKinney Basalt samples: plagioclase, olivine, and pyroxene. Locations were chosen based on surface morphology, as well as color, texture, or opacity. Previous studies note that this basalt contains some glass (Adcock et al., 2018); these locations produce Raman spectra that contain background noise and no other discernable signal. As such, while glass is present in our samples and may provide elements for reactions, we did not focus our Raman analyses on the glass since no discernable peaks appeared in the analyses, making it difficult to collect consistent and meaningful data. In a few instances where the CCD detector was oversaturated with signal from the Raman scattered light, the collection was aborted and repeated at 5% laser power.

We used Renishaw's WiRE 4.2 software to subtract the background noise and normalize the spectra. We analyzed each spectra further using *CrystalSleuth*, a free search engine software created by the RRUFF™ Project (Lafuente et al., 2015) that compares each spectrum to the library of Raman spectra in the RRUFF™ database. RRUFF™ files were compared to each spectrum and matches were based on the calculated similarity between spectra, regardless of the wavelength of laser used.

The complete sample collection process was repeated for the 3-month, 6-month, and 12-month observations. In addition, the 6-month extractions included two rough chips and one polished sample from each solution. We analyzed both the rough and polished surfaces with Raman spectroscopy. We also analyzed a polished control sample using a CAMECA SX100 electron probe micro-analyzer to determine the composition of the mineral phases (Table S1) using wavelength dispersive spectroscopy (WDS), and as a comparison to previously published bulk chemistry analyses (Adcock et al., 2018). We also collected backscatter electron (BSE) images to investigate the texture of the sample (Fig. 1) and identify targets for wavelength dispersive spectroscopy (WDS) analysis.

3. Results

Raman spectra of the brines showed no measurable changes throughout the experiment. From the control sample to the final sample, no additional peaks were observed in the brine samples analyzed, nor were there any alterations to the peak height, width, or position for any of the brine solute peaks. Because of this evidence, we focus on basalt alteration throughout the remainder of this study.

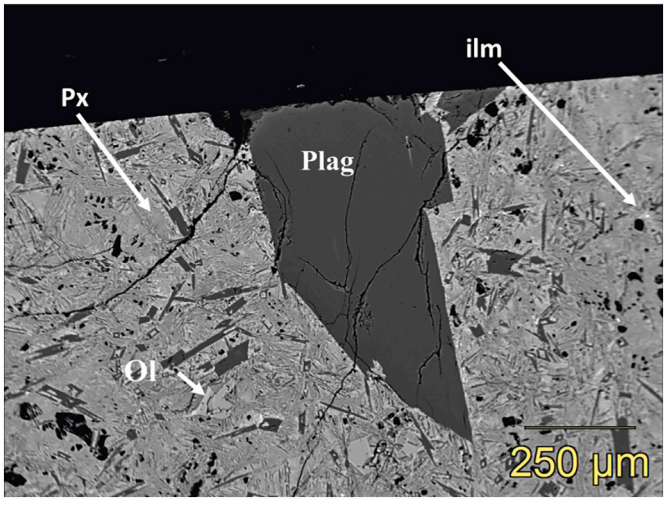

Fig. 1. BSE image of a control sample of the McKinney Basalt. A large plagioclase (Plag) crystal is centered with many smaller plagioclase crystals throughout the basalt. Small olivine (Ol) crystals are of a light gray color and pyroxene (Px) make up the rest of the matrix of the basalt. Tiny bright spots on the right side of the large plagioclase crystal are ilmenite (ilm). The pyroxene shows exsolution throughout the matrix and is particularly prevalent near the plagioclase crystals.

3.1. Control samples

We analyzed a control sample of the McKinney Basalt using a Rigaku Ultima-IV X-ray diffractometer and analyzed the diffraction data with MDI Jade to determine the bulk mineralogy of the rock before brine alteration. The phases identified in the electron microprobe analyses align closely with the phases also observed with powder X-ray diffraction (XRD) analysis and in the Raman spectra. XRD analysis (Table S2) of a micronized portion of our McKinney Basalt sample suggests the basalt is composed of plagioclase that closely fits with labradorite (55.9 wt%), forsterite (26.3 wt%), and an iron-bearing pyroxene similar to ferroan hedenbergite that makes up 12.6% of the sample. All three of these minerals were also observed in the Raman spectra collected from each sample. Ilmenite (3.0%) and quartz (1.3%) were also indicated in the XRD analysis but were not observed in the Raman spectra collected from the control sample.

Raman spectroscopy of the control sample also shows three main minerals in the McKinney Basalt sample: pyroxene, plagioclase, and olivine (Fig. 2 & Table 1). Olivine has a pair of intense peaks at 819 cm^{-1} and 850 cm^{-1}; plagioclase has a primary peak at 508 cm^{-1} and a secondary peak at 483 cm^{-1}. The unreacted sample from McKinney Basalt shares a minor peak with a plagioclase from the RRUFF™ database at 407 cm^{-1}, but lacks the sharp, minor peaks in the <400 wavenumbers range. The Raman spectra of pyroxene from the unreacted sample has a primary peak at 679–680 cm^{-1} (Fig. 2). The spectra from the RRUFF™ database shows a narrower peak in this spectral range of 678–680 cm^{-1}, while the basalt sample exhibits a broader curve. Similar broadness in pyroxene spectra has been attributed to natural impurities in previous studies (Vandenabeele, 2013). Backscatter electron imaging of the control polished sample supports this assertion as the pyroxene matrix shows exsolution throughout the sample (Fig. 1) which suggests the peak broadening observed in the pyroxene is likely due to variations in the chemistry between two or more exsolved pyroxene phases. (See Table 2.)

No Raman spectra indicative of ilmenite were collected from the control samples; XRD analysis suggests that this mineral accounts for about 3.0% of the basalt samples by weight. Therefore, it is within reason that any ilmenite in the control samples were either too small to be resolved or that no sample of ilmenite was found on the surface of the sample for Raman analysis (table S2). Ilmenite was observed in the electron microprobe analysis as a small, bright trace phases in BSE images. Quartz was only observed with the XRD. No evidence of quartz was detected with Raman or in the electron microprobe analyses of the control sample.

We collected 67 spot analysis spectra of the primary minerals on the surface of the control chip. No secondary minerals (iron oxides, sulfates, or carbonates) were observed in any of the analyses of the unreacted control sample

3.2. One month samples

The primary minerals olivine, pyroxene, and plagioclase observed from this reaction period did not show changes in the peak position nor peak intensities (Fig. S1). The basalt chips reacting in Na-ClO_4-H_2O produced spectra consistent with lepidocrocite and goethite (Fig. 3). An iron oxide spectrum was also observed on the McKinney Basalt chip taken from the ultra-pure water reactor. This spectrum is unique in that it contains the peak positions of both hematite and quartz, suggesting the deposition of the hematite onto a quartz crystal original to the basalt or co-precipitation of secondary hematite and quartz (Fig. 3). Spectra consistent with hematite were also observed on the basalt chips reacted

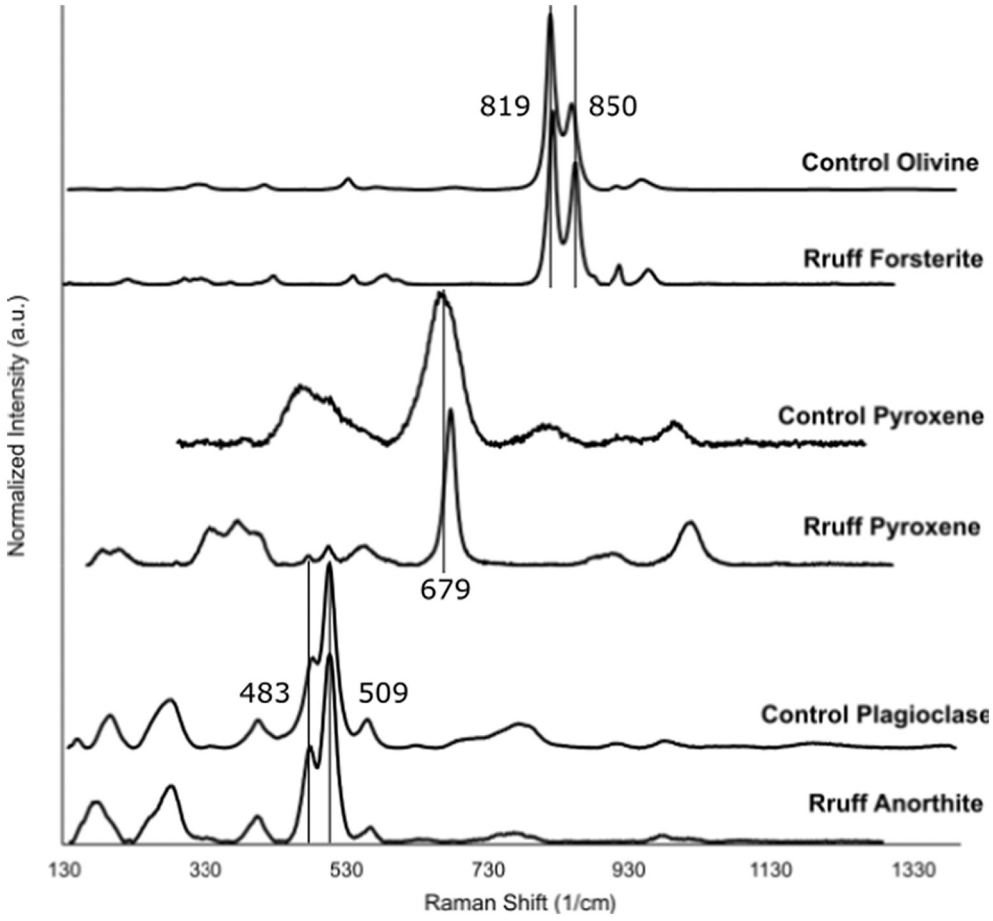

Fig. 2. Raman spectra of plagioclase, pyroxene, and olivine from a control sample of the McKinney Basalt as compared to spectra of anorthite, pyroxene, and forsterite from the online database RRUFF™.

Table 1
Raman peak positions of primary minerals in the McKinney Basalt samples. Units are in wavenumbers (cm^{-1}) and are based on spectra produced by a 532 nm green laser. Bold values denote a primary peak and all peak values are roughly located where the peak would be located within the spectrum.

Mineral	Raman excitation positions (cm^{-1})						
pyroxene				466	**679**		
olivine				534		**819**	**850**
plagioclase	196	278	407	**483**	**509**	562	
ilmenite	240	325	445			**680**	
augite	324	390			**665**		1008

in the Na-SO_4-H_2O brine. Chips reacted with Mg-Cl-SO_4-H_2O brine also produced spectra consistent with lepidocrocite ($Fe^{3+}O(OH)$). (Fig. 3).

Raman spectra consistent with sulfate minerals were also observed after 1 month of reaction (Fig. S2). A spectra matching thenardite (Na_2SO_4) was identified from a basalt chip reacting in the Na-ClO_4-SO_4-H_2O brine. Additionally, one spectrum collected from the McKinney basalt samples reacting in the Mg-Cl-SO_4-H_2O brine shows a good match to the sorosilicate, aluminum rich phase macfallite (Fig. S3) ($Ca_2(Mn^{3+}, Al)_3(SiO_4)(Si_2O_7)(OH)_3$) (Moore et al., 1979).

3.3. Three month samples

Raman spectra of the three primary minerals in our McKinney Basalt sample remained unchanged in all nine of the solutions (Fig. S4). Iron oxide secondary minerals appear more prominently in samples reacting in Na-ClO_4-H_2O brine, with samples producing spectra consistent with goethite, lepidocrocite, and hematite. A broad peak around 1350 cm^{-1} is present due to secondary phonon excitation of the iron oxides. This peak is not recorded in the RRUFF™ database since the RRUFF™ spectra terminate at 1300 wavenumbers, so the peak intensity is partially obstructed and likely misinterpreted as background noise. Faria (1997) shows this peak at 1350 wavenumbers as indicative of maghemite (Fig. S11). The Na-ClO_4-H_2O basalt sample shows evidence of hematite, but also shows a peak at 952 cm^{-1}, which matches well with hydroxyapatite ($Ca_{10}(PO_4)_6(OH)_2$). Finally, one sample reacting in Mg-SO_4-H_2O brine shows hematite along with quartz.

Sulfate minerals in addition to thenardite were also identified in the three month experiments. While thenardite is identified on a basalt chip reacting with Na-SO_4-H_2O brine with a peak at 991 cm^{-1} alone as well as in a spectra indicative of plagioclase, a peak at 985 cm^{-1} that closely fits with the peak intensity of epsomite ($MgSO_4{\cdot}7H_2O$) was observed in samples after reacting in Mg-SO_4-H_2O brine as well as the Mg-Cl-SO_4-H_2O brine (Fig. S6). A sample reacting in Ca-Cl-H_2O also produced a spectrum that contains a peak at 1010 cm^{-1}, which is the most intense peak for gypsum.

Carbonate minerals were also identified on the samples collected during this time interval (Fig. 4). Samples reacting in Mg-SO_4-H_2O, Mg-Cl-H_2O, and Na-Cl-H_2O each show a peak at 1086 cm^{-1} which fits with calcite. The calcite peak was also observed in a spectrum with olivine collected from a sample reacted with Na-Cl-H_2O brine, as well as in a spectrum with pyroxene collected from the Mg-Cl-H_2O experiment.

One spectrum collected from the basalt reacting in the ultra-pure water for three months shows a good fit for opal (Fig. 5), with an intense primary peak at 1001 cm^{-1}. The spectra also shows a secondary peak at 1030 cm^{-1}. Other smaller secondary peaks are ether absent or

Table 2
Summary of secondary minerals identified.

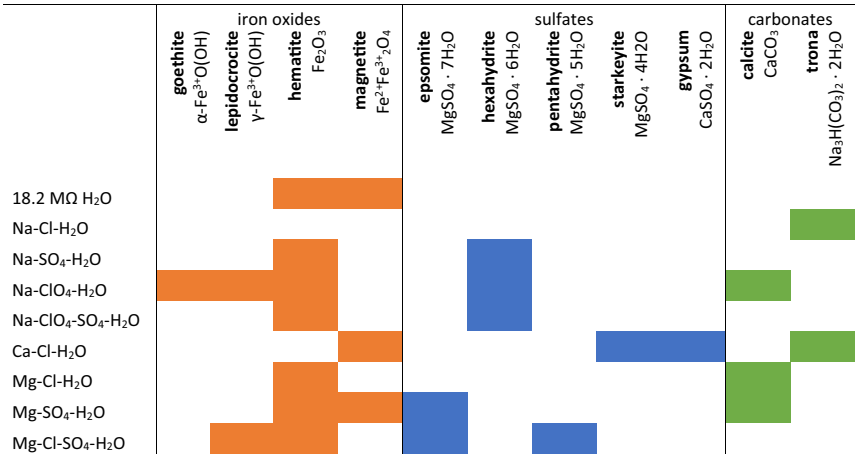

unable to be discerned from the background noise.

3.4. Six month samples

Chips reacting with brines containing magnesium cations produced peaks similar to those reacted with sodium-bearing brines. However, *Crystalsleuth* shows a higher match percentage with pentahydrate ($Mg(SO_4)\cdot 5H_2O$) in magnesium sulfate and magnesium chloride brines, whereas a higher percent match is found with hexahydrite ($Mg(SO_4)\cdot 6H_2O$) in sodium perchlorate and sodium sulfate experiments. The difference in peak position for these two hydrated forms of $MgSO_4$ is 13 wavenumbers, with the primary sulfate peak observed at 984 cm^{-1} for hexahydrite and 997 cm^{-1} for pentahydrate (Fig. S7). Pentahydrite was also observed in a basalt sample from the Mg-Cl-SO_4-H_2O experiment without any primary mineral peaks present in the spectrum, providing enough clarity to identify the peak position from the sample. One spectrum collected from a sample reacted with Na-Cl-H_2O brine shows a clear peak consistent with trona ($Na_3(HCO_3)\cdot 2H_2O$) (Fig. 6).

3.5. Twelve month samples

During the final collection period, no changes were observed in the spectra collected from the primary minerals pyroxene, olivine, plagioclase, and ilmenite (Fig. S8). Additionally, no quartz was observed. We observed spectra consistent with iron oxides within this sampling period (Fig. S9), including hematite in the Mg-SO_4-H_2O, Na-ClO_4-SO_4-H_2O, and Mg-Cl-SO_4-H_2O near-saturated brines. Additional spectra indicative of carbonate minerals were collected from samples of the basalt which had reacted with the mixed Na-ClO_4-SO_4-H_2O brine and the Mg-SO_4-H_2O brine, with a peak at 1086 wavenumbers, which is indicative of calcite (Fig. 7).

Samples reacted in the Mg-SO_4-H_2O and the Mg-Cl-SO_4-H_2O brines continued to produce spectra that are best fit with pentahydrite (Fig. 8). Additional sulfate minerals were observed in spectra collected from samples reacted in Na-SO_4-H_2O; however, the best fit for these samples is either thenardite, aluminite ($Al_2SO_4(OH)_4\cdot 7H_2O$) or blödite ($Na_2Mg(SO_4)_2\cdot 4H_2O$). Each of these minerals exhibit a peak near 992 cm^{-1}. However, since only a few secondary peaks are present in the spectra, it is difficult to discern the mineral species more precisely. The Na-ClO_4-H_2O brine experiments include spectra indicative of the alunite ($KAl_3(SO_4)_2(OH)_6$) (Fig. 8). (See Fig. 9.)

Three additional spectra from the twelve-month sampling period exhibit peaks that are not synonymous with the primary minerals, nor are they a good match with any of the iron oxides, carbonates or sulfates observed in the other samples. A spectrum of basalt reacted in Na-Cl-H_2O brine shows a major peak at 145 cm^{-1} and minor peaks at 320 cm^{-1}, 450^{-1}, and 675 cm^{-1} which is similar to anatase (TiO_2, Fig. S10). A spectrum from the basalt samples that reacted in Na-ClO_4-H_2O brine for 12 months shows a peak at 951 cm^{-1}, similar to either vivianite ($Fe_3^{2+}(PO_4)_2\cdot 8H_2O$) or ludlamite ($Fe_3^{2+}(PO_4)_2\cdot 4H_2O$) as well as peaks indicative of olivine. This observation, however, is not a complete match in the database to either phosphate mineral.

3.6. Overall patterns observed

We note that sulfate minerals were commonly observed in spectra of basalt that reacted in sulfate bearing solutions at all stages of the experiments, as well as rare observations in spectra collected from basalt that reacted with non-sulfate bearing solutions. However, perchlorate minerals were not observed in any of the spectra, including spectra collected from basalt chips that had reacted with near saturated perchlorate brine. Instead, the most common secondary mienrals observed in the basalt-Na-ClO_4-H_2O experiments are hematite, calcite, goethite, and anatase (Fig. S55).

4. Discussion

The McKinney Basalt chip samples exhibit qualitative evidence of alteration and secondary mineral formation in all solutions based on Raman observations of iron oxides, sulfates, carbonates, and opal, which were not observed in the control samples. Spectra consistent with iron oxides were commonly observed in both the one- and three-month experiments, indicating that iron oxides are likely evidence of early-stage basalt alteration in brines (Fig. S57). Throughout all the sampling intervals, iron oxide minerals were observed more frequently in samples reacted with ultra-pure water and sulfate-bearing brines than in the other solutions(Fig. S48-S56). This preferential precipitation is likely due to three mechanisms. First, perchlorate solutions may result in a slower release of iron than ultra-pure water and chloride solutions, similar to trends observed in jarosite dissolution experiments (Legett et al., 2018). Second, chloride solutions tend to maintain iron complexes in solution, resulting in less iron oxide precipitations as suggested by Phillips-Lander et al. (2019). Third, water activity could be a driving force of this phenomenon as Na-SO_4-H_2O brine and Mg-SO_4-H_2O brine have a water activity of 0.92 and 0.96, respectively (Guendouzi et al., 2003). The water activities of Na-Cl-H_2O, Ca-Cl-H_2O, Mg-Cl-H_2O, and Na-ClO_4-H_2O brines are significantly lower- 0.75, 0.2, 0.32, and 0.68, respectively (Ally, 1999; Chan and Ha, 1999; Morales et al., 2011). The

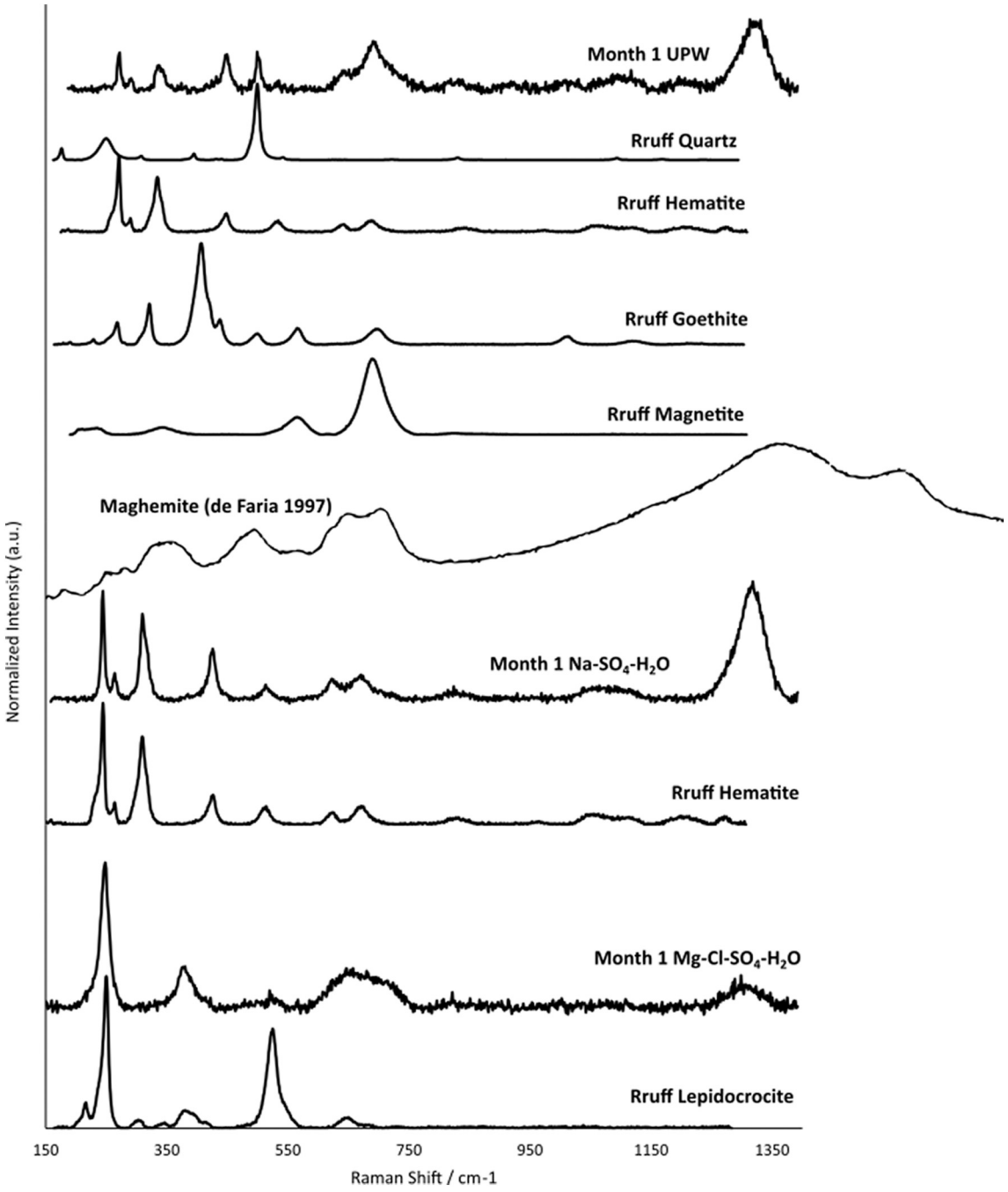

Fig. 3. Raman spectra of iron oxides identified on samples of McKinney Basalt as compared to known iron oxides from the online database RRUFF™. Samples collected in this experiment are denoted by the month collected and what solution the chips were reacting with. The spectra from this experiment include an artifact from the laser around 1340 wavenumbers.

disparity of the water activities may alter the rate at which iron dissolves into solution or precipitates as secondary minerals, as previous studies suggest a general trend of decreasing mineral dissolution rates as activity of water decreases (e.g. Steiner et al., 2016).

As the experiments continued, more spectra contained peaks indicative of hydrated sulfate minerals than iron oxides (Figs. S57–S60). In some cases, the sulfate phases may be attributed to brine residue remaining on the surface of the sample after rinsing (e.g., pentahydrate observed in samples reacted with Mg-SO_4-H_2O brines and thernadite observed in samples reacted with brines containing Na-SO_4-H_2O). These observations indicate that even if little alteration has occurred, sediments and rocks may contain traces of previous sulfate-bearing fluids present in the system, similar to the observed salts found within the fractures of Mars meteorite samples found on Earth (Bridges et al., 2001; Leshin and Vicenzi, 2006; Ling and Wang, 2015). However, evidence of the perchlorate brine was not evident in the Raman spectra suggesting that near-saturated perchlorate brine is much easier to remove from basalt surfaces via rinsing compared to near-saturated sulfate bearing brines. Therefore, subsequent fluid interactions may preferentially remove perchlorate salts while sulfate salts are more likely to remain on the rock surface. The rinsing procedure may have also removed other soluble phases weakly adsorbed to the basalt surface, but Raman spectroscopy of the filtered brines did not show evidence of any additional phases or ions in solution separate from the original brine chemistry.

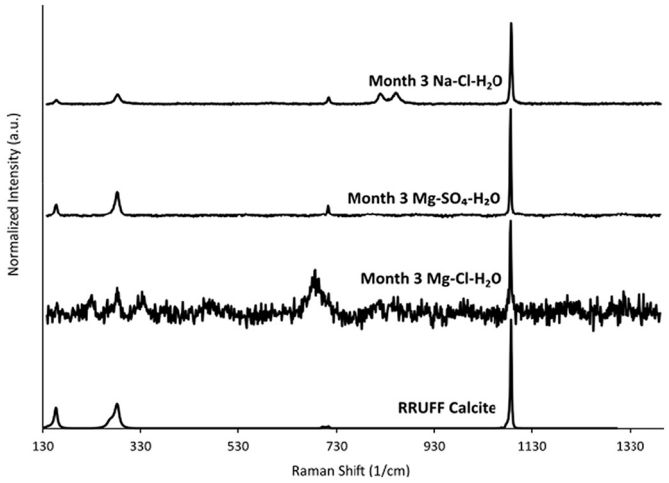

Fig. 4. Raman spectra of McKinney Basalt chips from the Snake River Lava flows after reacting in near-saturated brines for three months, as compared to the Raman spectra of calcite from the online RRUFF™ database. Each spectrum shows a primary peak at 1086 wavenumbers, which corresponds to the location of calcite excited by a 532 nm laser.

Sulfate minerals were also observed in samples reacted with brines that did not contain sulfate anions (e.g., alunite observed in the twelve-month Na-ClO_4-H_2O brine experiment). Spectra indicative of blödite or aluminite in the Na-SO_4-H_2O brine also indicate that sulfate brine-mineral interactions can leach additional cations from the sample, resulting in formation of new sulfate phases.

The identification of sulfates in the experiments reacted with Cl^- and ClO_4^- brines (i.e., brines that did not contain sulfate) requires a sulfur source within the basalt samples. However, neither sulfate nor sulfide

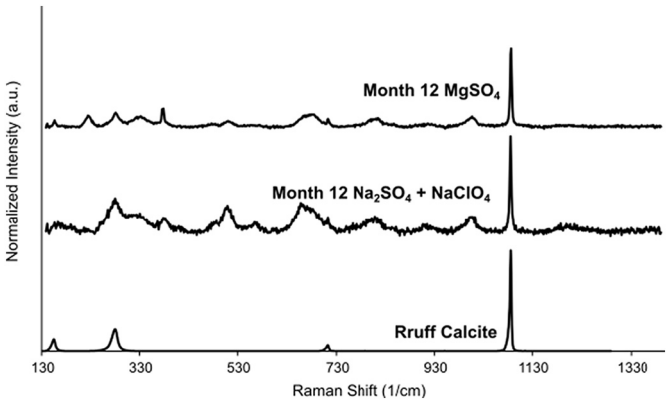

Fig. 7. Raman spectra of KcKinney basalt from the Snake River Lava flows as compared to calcite from the online Rruff™ database. The basalt samples had been reacting in a near-saturated brine of $MgSO_4$ or a Na-ClO_4-SO_4H_2O brine for twelve months.

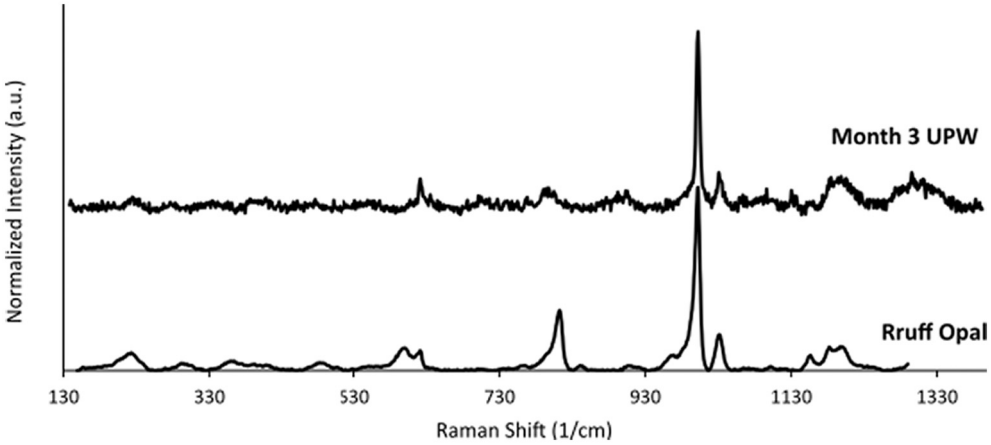

Fig. 5. Raman spectra of a McKinney Basalt chip from the Snake River Lava flows after reacting in ultra-pure water for three months, as compared to the spectra of opal from the online RRUFF™ database.

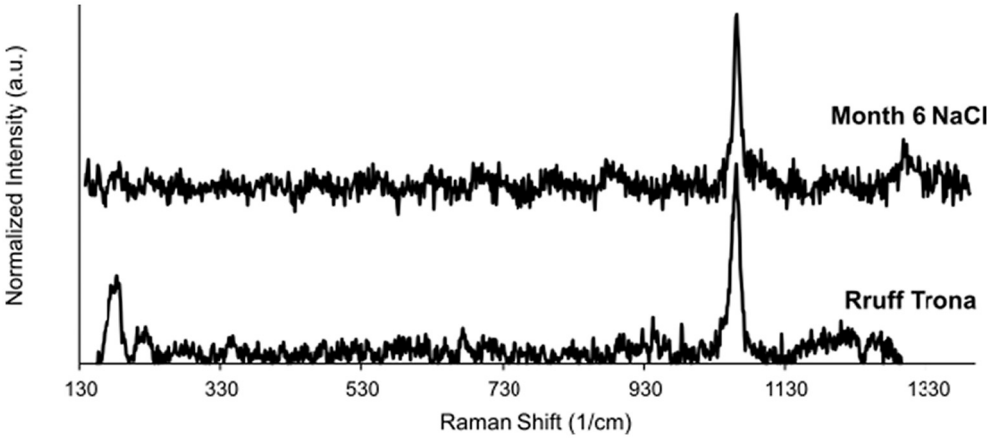

Fig. 6. Raman spectra of a KcKinney Basalt from the Snake River Lava flows as compared to a spectrum of trona from the online RRUFF™ database.

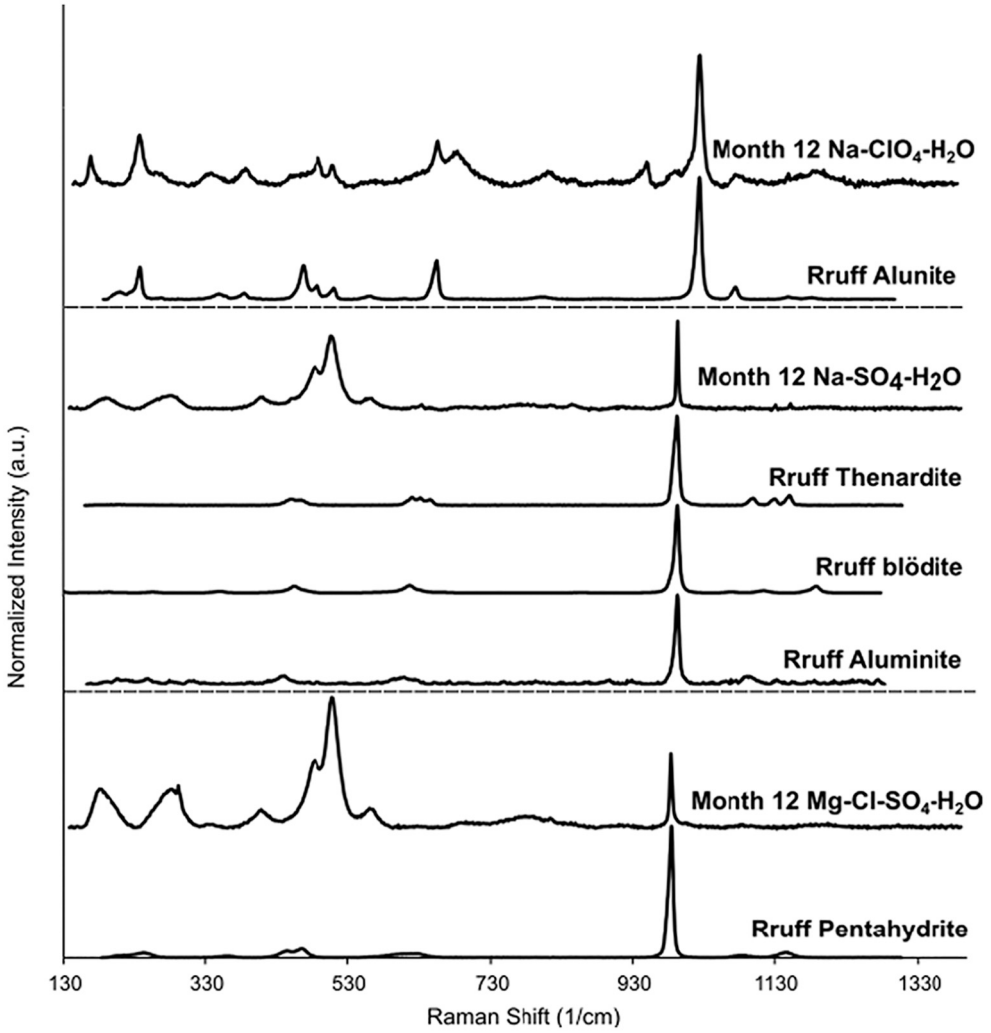

Fig. 8. Raman spectra of McKinney Basalt samples from the Snake River Lava flows as compared to sulfate minerals from the online RRUFF™ database. The spectra from the two samples reacting in the Na-SO_4-H_2O brine and the Mg-Cl-SO_4-H_2O brine both exhibit additional peaks that are indicative of anorthite.

minerals were detected in the Raman spectra or XRD analyses of the control samples. In addition, EDS analysis of the control chip did not detect sulfur in the unreacted basalt samples. However, micron- or nano-scale sulfide minerals may have gone undetected in these analyses. The presence of sulfur, while not detected by our analyses of the control samples, has been observed in previous studies of McKinney Basalt (Adcock et al., 2018; Doc Richardson et al., 2012). Thus, we reason that sulfur is present in our samples but is below the detection limit of our instruments.

Indeed, bulk chemical analysis of the McKinney Basalt used in this study indicates 0.6 wt% loss on ignition (LOI), which is likely attributed to loss of adsorbed water and volatiles such as sulfur and carbon. Observations of sulfate minerals formed within the lava tube cave systems of the Blue Dragon Flow, part of the Snake River Plain basalts also suggest that there is a sulfur source within the primary rocks (Doc Richardson et al., 2012). Our observations of sulfate minerals formed from basalt interacting with chloride and perchlorate brines demonstrates how trace constituents within the basalt samples can be preferentially leached and precipitate secondary minerals in near saturated brines, even if those constituents may be below typical detection limits for bulk chemistry.

The identification of carbonates is also interesting, since no carbon or carbonate phases were detected in the XRD or EDS analyses of the control samples, nor are carbonates reported in previous studies of McKinney basalt. The source of carbon needed to form the secondary carbonates may be CO_2 from the atmosphere trapped within the reactor bottles, that then dissolve into solution. Previous studies show evidence of carbonate solubility decreasing as the system becomes more saline, causing carbonate minerals to precipitate (Hänchen et al., 2008; Kim et al., 2017; Papadimitriou et al., 2004). This indicates that trace carbonate minerals observed with Raman spectroscopy can also provide clues about the atmospheric composition during the weathering period (Bonales et al., 2013; Eytan Sass and Ben-Yaakov, 1977; Moyano-Cambero et al., 2017; Papadimitriou et al., 2004). Indeed, observations of carbonates in this study is of interest as evidence of carbonate species have been identified from orbiters and possible water-rock interactions that produce carbonates can be broadened to include hypersaline solutions (Ehlmann et al., 2008; Horgan et al., 2019).

Many carbonate minerals, like the sulfates, exhibit a consistent spectrum shape of a single, intense peak that is shifted by a few wavenumbers from that of carbonate ions in aqueous solutions. Carbonate species dissolved in solution will produce a peak at 1064 wavenumbers, while carbonate minerals with different cations and varying hydration states show a shift in the carbonate ion peak from 1085 cm^{-1} in rhodochrosite ($Mn(CO_3)$) to 1122 cm^{-1} in huntite ($CaMg_3(CO_3)_4$) (Martinez et al., 2004). With few exceptions– such as dolomite, siderite, and magnesite– the only discernable peak is the single, intense carbonate peak between ~1080–1125 cm^{-1} (Fig. 10).

It is important to note that the secondary minerals observed in this study can, and often are, formed by by less saline solutions on Earth. Our

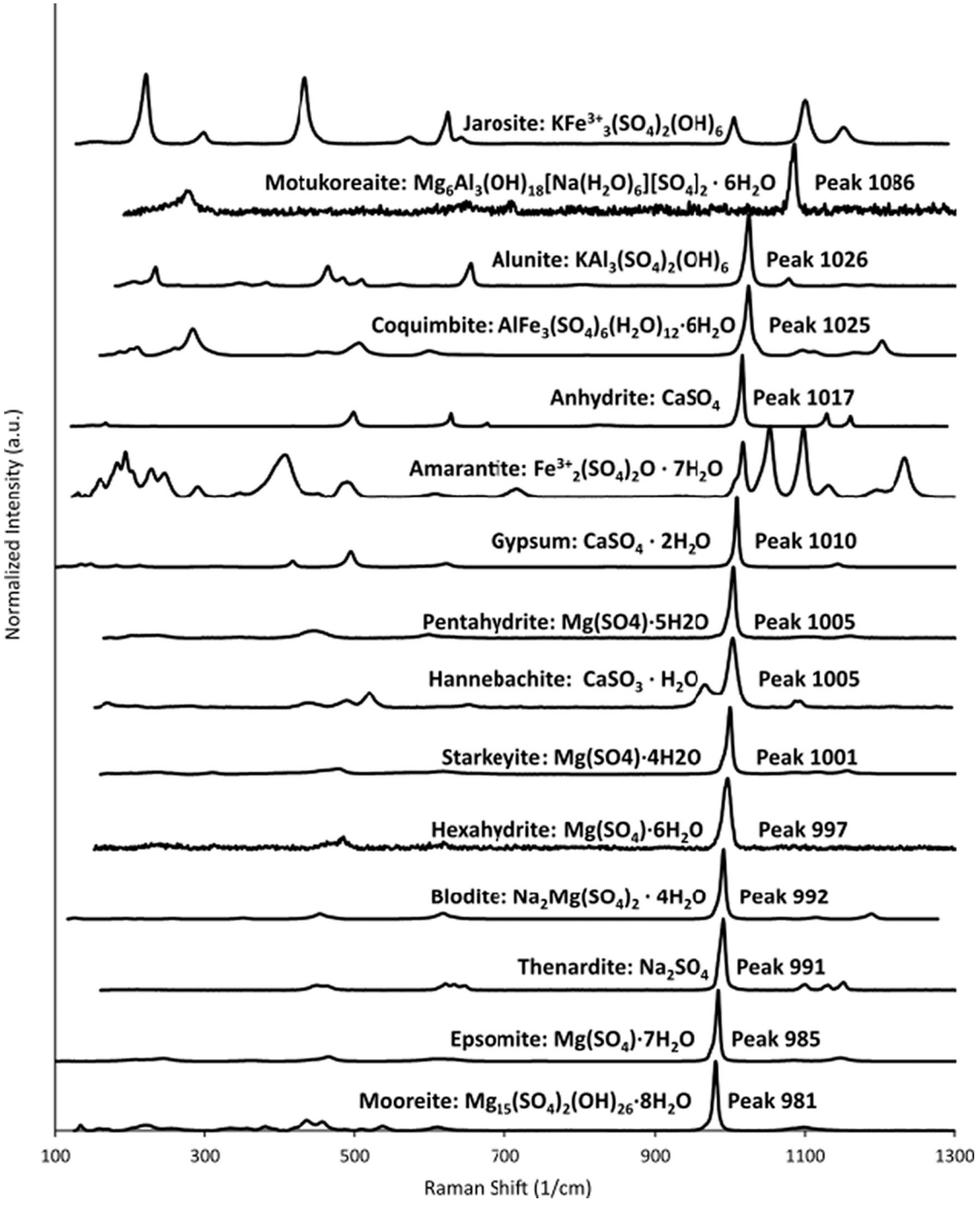

Fig. 9. Raman spectra of select sulfate minerals. Data is from the online RRUFF™ database.

focus on highly saline solutions is to ascertain the products of basalt alteration based on our hypothesis that any recent liquid water present on the surface of Mars is likely present as a near-saturated brine formed as liquid water deliquesces, evaporates, or freezes on the Martian surface. However, our focus on secondary mineral formation on the basalt surface also required us to rinse the samples after reacting in the brines since any salt formation on the basalt would impede Raman spectroscopy. Trace amounts of more soluble secondary materials were likely lost in the process; however, rinsing allows us to focus on the less soluble secondary minerals that are more likely to be preserved in the rock record over geologic time.

4.1. Implications

Of the 2379 total Raman spectra collected in these experiments, ~88% showed peaks indicative of at least one of the primary minerals, while ~12% contained peaks consistent with secondary mineral formation (Fig. 11). Therefore, when using a focused laser spot size (~5–10 μm) it is necessary to take multiple spectra within even a small area of a sample target if we are seeking evidence of secondary minerals indicative of aqueous alteration. Failure to take multiple spectra of a target risks collecting data that does not represent the diversity of phases present in the sample.

Raman spectroscopy can present challenges when the sample is dark

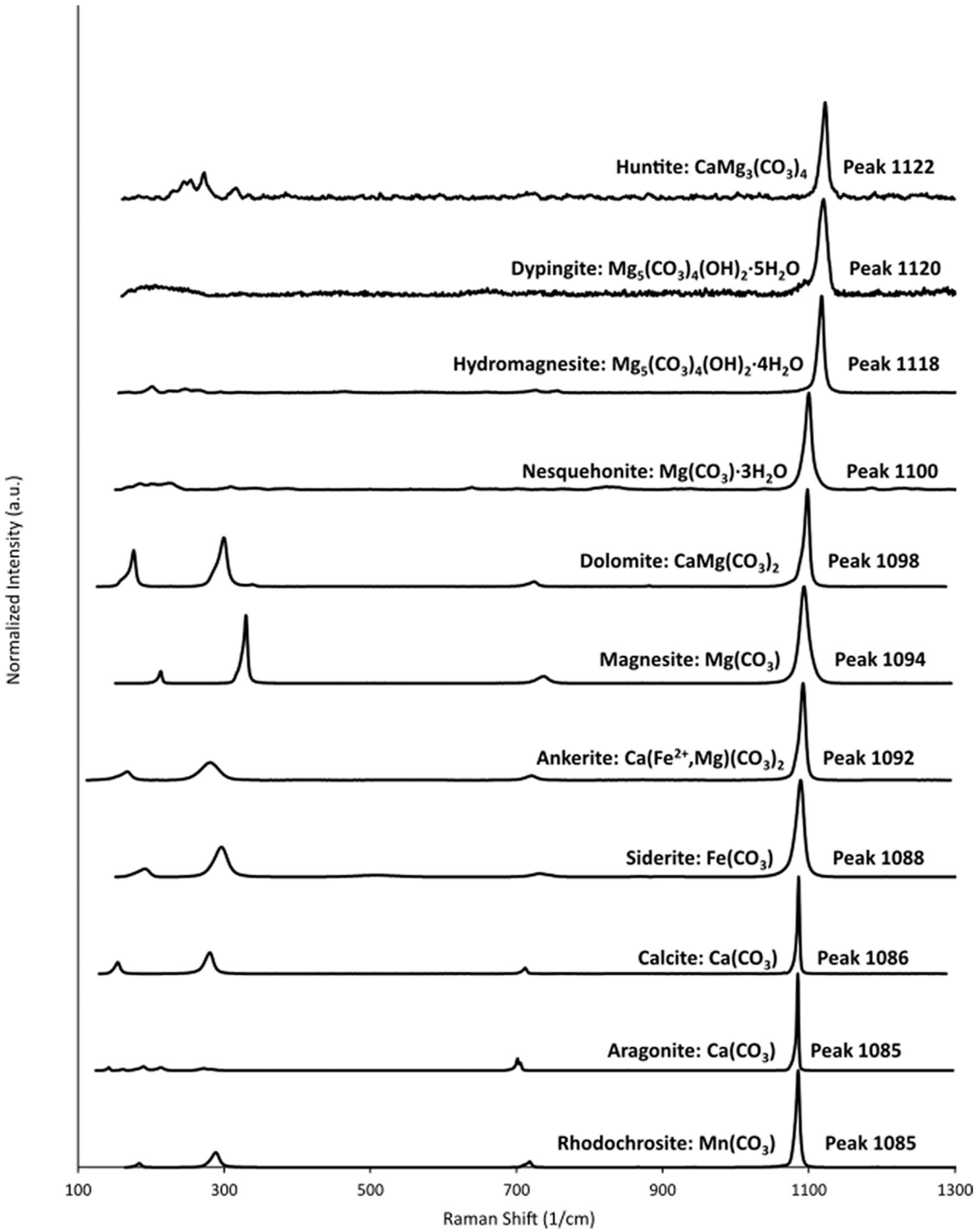

Fig. 10. Raman spectra of carbonate minerals from the online RRUFF™ database. Order is presented to ascend with increasing wavenumbers.

due to the ability for the laser to heat the sample. Laser heating of the sample can cause phase changes and burning. While the simple solution to this issue is to reduce the laser power, this power reduction must be countered with a longer total collection time to offset the background noise. Fluorescence is another common challenge in Raman spectroscopy, creating peaks and increased background signal that can obscure the primary Raman peaks. In some cases, fluorescence may even oversaturate the detector. In order to reduce fluorescence, investigators may use a laser with a longer wavelength.

Additional challenges occur in interpreting Raman spectra, as the signal produced by heterogeneous samples can be complex and the combination of peaks observed can be non-unique. Many phases produce spectra with multiple peaks, some of which may overlap with other phases. When using an automated search program, the algorithms may suggest geologic or organic phases unlikely to exist in the context of the experiments. However, careful analysis can allow for robust interpretations of spectra that contain multiple peaks.

Geochemical context is vital when a spectrum contains only shows one peak (e.g. sulfate, carbonate, trona) or multiple phases contain a peak or broad shoulder in the same location (e.g. pyroxene, goethite). In this case, the spectra for both pyroxene and goethite contain additional peaks that can be used to clearly identify which phase is present. This

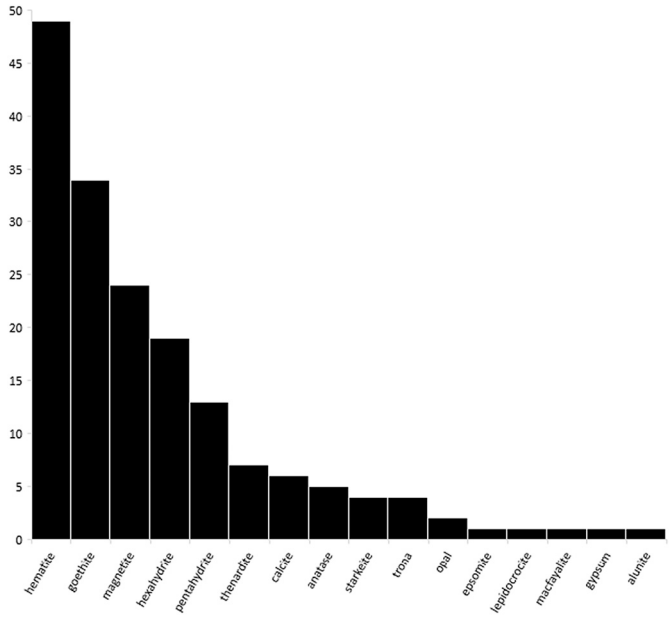

Fig. 11. Histogram of observed secondary minerals for all solutions for the entirety of the experiment.

deductive technique of identification through elimination of known phases is particularly effective when a researcher limits their scope to the geologic context of the sample. For example, our observations of a strong carbonate peak in several samples was at first surprising, but careful consideration of the geochemical context of the experiments and an examination of the literature indicate that carbonate precipitation is possible. In addition, peaks produced by carbonate minerals (1085–1122 wavenumbers) are significantly shifted away from other anion peaks which might be more expected in these experiments, such as sulfate phases (980–1026 wavenumbers) and perchlorate (928 cm^{-1}). Due to these differences in peak position, as well as the clear, intense peaks observed at 1086, these peaks are likely formed by carbonate minerals, since no other mineral phases in the database produces intense single peaks in this region.

In addition, the Raman intensity of peaks is also important to consider. Our assessment that $NaClO_4$ was not observed is supported by previous experiments that demonstrate the very high intensity of the perchlorate peak both in solution and as a solid phase (Mason and Elwood Madden, 2022; McGraw et al., 2018). Employing geochemical context, as well as our understanding of the relative intensities of peaks expected from different phases aided our interpretations of the spectra matches produced by CrystalSleuth (Lafuente et al., 2015). The resulting list of possible phases in the spectrum is filtered using known geochemical constraints and geochemical context, laser wavelength, and finally fitness of the spectrum to the RRUFF™ library. We expect similar challenges to occur in the field, where heterogeneous samples will be the norm. Robust interpretations will rely upon both careful examination of peak positions and intensities, but also analysis of secondary peaks and attention to the geochemical and geologic context of the samples.

An alternate strategy could be to obtain a Raman spectrum of a larger sample area by using a less focused laser spot instead of a narrow point. This strategy would likely include more surface minerals in each spectrum. However, based on our experience in this study, intense peaks from more abundant primary minerals may outweigh a weaker signal from secondary minerals. For example, olivine produced intense peaks that dominated the spectra, making the signal from secondary phases more difficult to detect (Fig. 12). Since olivine is both abundant in the sample, and produces intense peaks, any additional minerals sampled within the focus area usually produced much less prevalent spectra compared to olivine, making it difficult to identify these secondary without multiple reviews of all the data.

The results of these experiments demonstrate that secondary carbonate minerals can form from the reaction of Mars analogous basalt and near-saturated brines under relatively short time spans. In our experiments, we interpret that atmospheric CO_2 was likely the main source of carbon needed for carbonate precipitation. Similar processes may have formed carbonates on the surface of Mars, and if such processes occurred, then Raman spectroscopy is a viable tool for identifying carbonate minerals present on the surface.

Previous studies have suggested that there is evidence of carbonates in the Martian dust and sediment based on orbital, lander, and rover observations (Boynton et al., 2007). This is in spite of evidence that Mars experienced highly acidic and oxidizing environments during the Hesperian (Dehouck et al., 2016, 2012; Fairen et al., 2004; Horgan et al., 2019; Kim et al., 2017; Moyano-Cambero et al., 2017; Saheb et al., 2011). If carbonate minerals are observed directly with the Raman spectrometer, this would provide support for a more neutral pH environment during the period of alteration and deposition. Since the primary peaks observed for carbonate minerals do not overlap with the primary peaks observed for sulfates, it is relatively straightforward to discern between the spectra of these two important mineral groups. The Renishaw In*Via* Raman spectrometer coupled with a 532 nm laser, as used in this study, has a spectral resolution of ~1.25 wavenumbers with the 1200 l/cm grating or ~ 0.75 wavenumbers with the 2400 l/cm grating. While the Raman spectrometer onboard Perseverance rover has

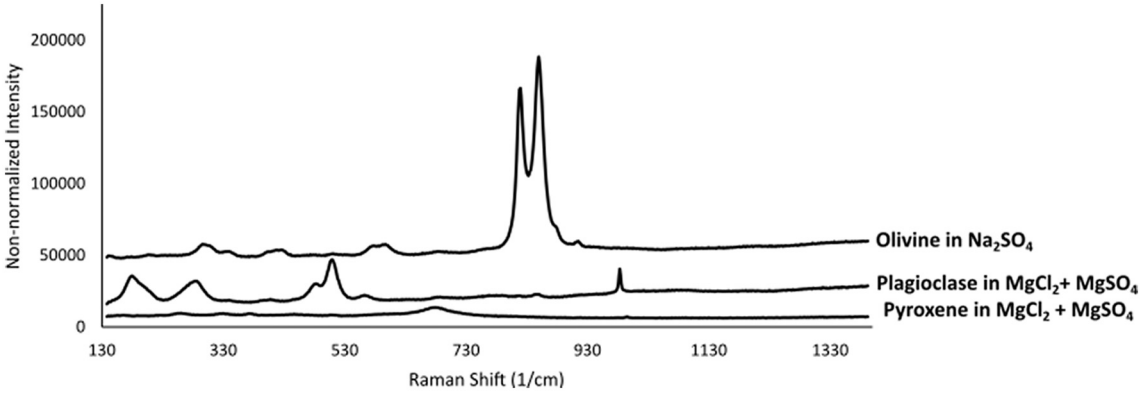

Fig. 12. Raman spectra of the three primary minerals before normalizing the intensities from a sample of KcKinney Basalt from the Snake River Lava flows. The plagioclase sample includes a secondary mineral peak at 997 cm^{-1} which signifies hexahydrite. While the hexahydrite peak is relatively intense as compared to the peaks for plagioclase and pyroxene, such a peak is not as well detected as the signal from olivine and risks being overlooked if the peak intensity of the secondary mineral were located within the peak range of olivine.

have a spectral resolution of about 4 wavenumbers (Wiens et al., 2017). While this spectral resolution providse enough clarity to discern whether a spectra is indicative of one of the broad mineral groups (e.g. sulfate, carbonate, and Mn/Fe-oxide minerals), it may be difficult to discern between specific mineral phases within a broader group, due to the slight changes in primary peak position indicative of individual carbonate, sulfate, and phosphate species within the broader group. Other analyses will likely be needed to further identify specific mineral phases.

5. Conclusions

These experiments suggest that secondary minerals created from the alteration of Mars analogous basalt in near-saturated brines can be observed with Raman spectroscopy. Key peaks can be used to identify the presence of secondary mineral groups based on the general location of a primary peak (e.g., primary peaks ranging 1080 cm^{-1} to 1130 cm^{-1} for carbonates, and 980 cm^{-1} to 1020 cm^{-1} for sulphate minerals). These general insights can lead scientists to further investigate an area with other, more resource intensive instruments to provide bulk chemistry and mineralogy of the sample. Based on this study, we expect that even with the limitations of a broad, low resolution spectrometer, a spectrum exhibiting a strong peak can be utilized to identify the mineral group, which may be helpful in constraining the conditions of alteration. However, multiple spectra may need to be collected over a fairly small sample area in order to capture secondary minerals phases that may be present, as only 12% of the spectra collected in this study contained evidence of secondary mineral phases. Such challenges, however, can easily be conquered with automation and is may be of little concern as the rocks on Mars would be altered for a longer period of time, increasing the likelihood of widespread secondary minerals. Thus, Raman is a useful, non-destructive measurement technique that provides opportunities for significant in situ research focused on secondary alteration minerals on the surface of Mars. The returned samples can be measured with the Raman spectrometer before any destructive processes as either complementary data or as an indicator for how to proceed with other measurements.

Declaration of Competing Interest

The authors declare that they have no known competing financial interests or personal relationships that could have appeared to influence the work reported in this paper.

Acknowledgements

This project was funded by NASA PDART grant 80NSSC18K0512. The authors wish to thank the NAI/APS Lewis and Clark Astrobiology Field scholarship, awarded to C. Phillips-Lander, for the funding to obtain the field samples. We also thank editor Debra Buczkowski, an anonymous reviewer,*V*. Chevrier, and K. Benison for very helpful comments that significantly strengthened this manuscript.

Appendix A. Supplementary data

Supplementary data to this article can be found online at https://doi.org/10.1016/j.icarus.2022.115111.

References

Abotalib, A.Z., Heggy, E., 2019. A deep groundwater origin for recurring slope lineae on Mars. Nat. Geosci. 12, 235–241. https://doi.org/10.1038/s41561-019-0327-5.

Adcock, C.T., Udry, A., Hausrath, E.M., Tschauner, O., 2018. Craters of the Moon National Monument basalts as unshocked compositional and weathering analogs for martian rocks and meteorites. Am. Mineral. 103, 502–516. https://doi.org/10.2138/am-2018-6193.

Ally, M.R., 1999. Solute and solvent activities of CaCl2(aq) solutions from the adsorption isotherm treatment. J. Chem. Eng. Data 44, 792–797. https://doi.org/10.1021/je980296c.

Baker, V.R., Strom, R.G., et al., 1991. Ancient oceans, ice sheets and the hydrological cycle on Mars. Nature (London) 352, 589.

Bakker, R.J., 2004. Raman spectra of fluid and crystal mixtures in the systems H2O, H2O–NaCl and H2O–MgCl2 at low temperatures: applications to fluid-inclusion research. Can. Mineral. 42, 1283–1314. https://doi.org/10.2113/gscanmin.42.5.1283.

Beck, A.W., Murchie, S.L., Viviano, C.E., 2020. A search for early- to mid-Noachian chloride-rich deposits on Mars. Icarus 338, 113552. https://doi.org/10.1016/j.icarus.2019.113552.

Beegle, L., Bhartia, R., White, M., DeFlores, L., Abbey, W., Wu, Yen-Hung, Cameron, B., Moore, J., Fries, M., Burton, A., Edgett, K.S., Ravine, M.A., Hug, W., Reid, R., Nelson, T., Clegg, S., Wiens, R., Asher, S., Sobron, P., 2015. SHERLOC: Scanning habitable environments with Raman & luminescence for organics & chemicals. In: 2015 IEEE Aerospace Conference. Presented at the 2015 IEEE Aerospace Conference. IEEE, Big Sky, MT, pp. 1–11. https://doi.org/10.1109/AERO.2015.7119105.

Benison, K.C., LaClair, D., Walker, J., 2008. Physical sedimentology experiments with sulfuric acid solutions: implications for Mars? Earth Planet. Sci. Lett. 270, 330–337. https://doi.org/10.1016/j.epsl.2008.03.036.

Bhattacharya, J.P., Payenberg, T.H.D., Lang, S.C., Bourke, M., 2005. Dynamic river channels suggest a long-lived Noachian crater lake on Mars. Geophys. Res. Lett. 32 https://doi.org/10.1029/2005GL022747.

Bish, D.L., William Carey, J., Vaniman, D.T., Chipera, S.J., 2003. Stability of hydrous minerals on the martian surface. Icarus 164, 96–103. https://doi.org/10.1016/S0019-1035(03)00140-4.

Bonales, L..J., Muñoz-Iglesias, V., Prieto-Ballesteros, O., 2013. Raman spectroscopy as a tool to study the solubility of CO₂ in magnesium sulphate brines: application to the fluids of Europa's cryomagmatic reservoirs. Eur. J. Mineral. 25, 735–743. https://doi.org/10.1127/0935-1221/2013/0025-2312.

Boynton, W.V., Taylor, G.J., Evans, L.G., Reedy, R.C., Starr, R., Janes, D.M., Kerry, K.E., Drake, D.M., Kim, K.J., Williams, R.M.S., Crombie, M.K., Dohm, J.M., Baker, V., Metzger, A.E., Karunatillake, S., Keller, J.M., Newsom, H.E., Arnold, J.R., Brückner, J., Englert, P.A.J., Gasnault, O., Sprague, A.L., Mitrofanov, I., Squyres, S. W., Trombka, J.I., d'Uston, L., Wänke, H., Hamara, D.K., 2007. Concentration of H, Si, Cl, K, Fe, and Th in the low- and mid-latitude regions of Mars. J. Geophys. Res. Planets 112. https://doi.org/10.1029/2007JE002887.

Brass, G.W., 1980. Stability of brines on Mars. Icarus 42, 20–28. https://doi.org/10.1016/0019-1035(80)90237-7.

Bridges, J.C., Catling, D.C., Saxton, J.M., Swindle, T.D., Lyon, I.C., Grady, M.M., 2001. Alteration assemblages in martian meteorites: implications for near-surface processes. Space Sci. Rev. 96, 365–392. https://doi.org/10.1023/A:1011965826553.

Carr, M.H., 1979. Formation of Martian flood features by release of water from confined aquifers. J. Geophys. Res. 84, 2995. https://doi.org/10.1029/JB084iB06p02995.

Carrier, B.L., Kounaves, S.P., 2015. The origins of perchlorate in the Martian soil. Geophys. Res. Lett. 42, 3739–3745. https://doi.org/10.1002/2015GL064290.

Carter, J., Poulet, F., Bibring, J.-P., Mangold, N., Murchie, S., 2013. Hydrous minerals on Mars as seen by the CRISM and OMEGA imaging spectrometers: updated global view. J. Geophys. Res. Planets 118, 831–858. https://doi.org/10.1029/2012JE004145.

Chan, C.K., Ha, Z., 1999. A simple method to derive the water activities of highly supersaturated binary electrolyte solutions from ternary solution data. J. Geophys. Res.-Atmos. 104, 30193–30200. https://doi.org/10.1029/1999JD900942.

Chevrier, V.F., Morisson, M., 2021. Carbonate-phyllosilicate parageneses and environments of aqueous alteration in Nili fossae and Mars. J. Geophys. Res. Planets 126, e2020JE006698. https://doi.org/10.1029/2020JE006698.

Chevrier, V.F., Rivera-Valentin, E.G., 2012. Formation of recurring slope lineae by liquid brines on present-day Mars: LIQUID BRINES ON MARS. Geophys. Res. Lett. 39, n/a-n/a. https://doi.org/10.1029/2012GL054119.

Chevrier, V.F., Hanley, J., Altheide, T.S., 2009. Stability of perchlorate hydrates and their liquid solutions at the Phoenix landing site. Mars. Geophys. Res. Lett. Wash. 36 https://doi.org/10.1029/2009GL037497.

Chevrier, V.F., Rivera-Valentín, E.G., Soto, A., Altheide, T.S., 2020. Global temporal and geographic stability of brines on present-day Mars. Planet. Sci. J. 1, 64. https://doi.org/10.3847/PSJ/abbc14.

Chou, I.-M., Wang, A., 2017. Application of laser Raman micro-analyses to Earth and planetary materials. J. Asian Earth Sci., Asian Orogeny and Continental Tectonics from Geochemical Perspectives, A Special Issue in Memory of Professor Bor-ming Jahn for His Scientific Contributions and Service (Part I) 145, 309–333. https://doi.org/10.1016/j.jseaes.2017.06.032.

Clark, B.C., Baird, A.K., 1979. Volatiles in the Martian regolith. Geophys. Res. Lett. 6, 811–814. https://doi.org/10.1029/GL006i010p00811.

Clifford, S.M., Parker, T.J., 2001. The evolution of the martian hydrosphere: implications for the fate of a Primordial Ocean and the current state of the Northern Plains. Icarus 154, 40–79. https://doi.org/10.1006/icar.2001.6671.

Cull, S.C., Arvidson, R.E., Catalano, J.G., Ming, D.W., Morris, R.V., Mellon, M.T., Lemmon, M., 2010. Concentrated perchlorate at the Mars Phoenix landing site: evidence for thin film liquid water on Mars: PHOENIX-CONCENTRATED PERCHLORATE. Geophys. Res. Lett. 37, n/a–n/a. https://doi.org/10.1029/2010GL045269.

Das, S., Hendry, M.J., 2011. Application of Raman spectroscopy to identify iron minerals commonly found in mine wastes. Chem. Geol. 290, 101–108. https://doi.org/10.1016/j.chemgeo.2011.09.001.

Dehouck, E., Chevrier, V., Gaudin, A., Mangold, N., Mathé, P.-E., Rochette, P., 2012. Evaluating the role of sulfide-weathering in the formation of sulfates or carbonates

on Mars. Geochim. Cosmochim. Acta 90, 47–63. https://doi.org/10.1016/j.gca.2012.04.057.
Dehouck, E., Gaudin, A., Chevrier, V., Mangold, N., 2016. Mineralogical record of the redox conditions on early Mars. ICARUS 271, 67–75. https://doi.org/10.1016/j.icarus.2016.01.030.
Doc Richardson, C., Hinman, N.W., McHenry, L.J., Michelle Kotler, J., Knipe, D.L., Scott, J.R., 2012. Secondary sulfate mineralization and basaltic chemistry of craters of the Moon National Monument, Idaho: potential martian analog. Planet. Space Sci. 65, 93–103. https://doi.org/10.1016/j.pss.2012.02.002.
Dove, P.M., Han, N., De Yoreo, J.J., 2005. Mechanisms of classical crystal growth theory explain quartz and silicate dissolution behavior. Proc. Natl. Acad. Sci. U. S. A. 102, 15357–15362.
Ehlmann, B.L., Mustard, J.F., Murchie, S.L., Poulet, F., Bishop, J.L., Brown, A.J., Calvin, W.M., Clark, R.N., Des Marais, D.J., Milliken, R.E., Roach, L.H., Roush, T.L., Swayze, G.A., Wray, J.J., 2008. Orbital identification of carbonate-bearing rocks on Mars. Science 322, 1828–1832.
Fairen, A.G., Fernandez-Remolar, D., Dohm, J.M., Baker, V.R., Amils, R., 2004. Inhibition of carbonate synthesis in acidic oceans on early Mars. Nature (London) 431, 423–426 https://doi.org.ezproxy.lib.ou.edu/10.1038/nature02911.
Faria, D.L.A. de, 1997. Raman microspectroscopy of some iron oxides and oxyhydroxides. J. Raman Spectrosc. https://doi.org/10.1002/(SICI)1097-4555(199711)28:11<873::AID-JRS177>3.0.CO;2-B.
Frezzotti, M.L., Tecce, F., Casagli, A., 2012. Raman spectroscopy for fluid inclusion analysis. J. Geochem. Explor. 112, 1–20. https://doi.org/10.1016/j.gexplo.2011.09.009.
Gaillard, F., Michalski, J., Berger, G., McLennan, S.M., Scaillet, B., 2013. Geochemical reservoirs and timing of sulfur cycling on Mars. Space Sci. Rev. 174, 251–300. https://doi.org/10.1007/s11214-012-9947-4.
Goudge, T.A., Fassett, C.I., Head, J.W., Mustard, J.F., Aureli, K.L., 2016. Insights into surface runoff on early Mars from paleolake basin morphology and stratigraphy. Geology 44, 419–422. https://doi.org/10.1130/G37734.1.
Guendouzi, M.E., Mounir, A., Dinane, A., 2003. Water activity, osmotic and activity coefficients of aqueous solutions of Li2SO4, Na2SO4, K2SO4, (NH4)2SO4, MgSO4, MnSO4, NiSO4, CuSO4, and ZnSO4 at T=298.15K. J. Chem. Thermodyn. 35, 209–220. https://doi.org/10.1016/S0021-9614(02)00315-4.
Haberle, R.M., McKay, C.P., Schaeffer, J., Cabrol, N.A., Grin, E.A., Zent, A.P., Quinn, R., 2001. On the possibility of liquid water on present-day Mars. J. Geophys. Res. Planets 106, 23317–23326. https://doi.org/10.1029/2000JE001360.
Hänchen, M., Prigiobbe, V., Baciocchi, R., Mazzotti, M., 2008. Precipitation in the mg-carbonate system—effects of temperature and CO2 pressure. Chem. Eng. Sci. 63, 1012–1028. https://doi.org/10.1016/j.ces.2007.09.052.
Hanley, J., Chevrier, V.F., Mellon, M., Anonymous, 2013. Distribution, detection, and implications of chlorine salts on Mars. Abstr. Pap. Submitt. Lunar Planet. Sci. Conf. 44. Paper 2923.
Haskin, L.A., Wang, A., Jolliff, B.L., McSween, H.Y., Clark, B.C., Des Marais, D.J., McLennan, S.M., Tosca, N.J., Hurowitz, J.A., Farmer, J.D., Yen, A., Squyres, S.W., Arvidson, R.E., Klingelhöfer, G., Schröder, C., de Souza, P.A., Ming, D.W., Gellert, R., Zipfel, J., Brückner, J., Bell, J.F., Herkenhoff, K., Christensen, P.R., Ruff, S., Blaney, D., Gorevan, S., Cabrol, N.A., Crumpler, L., Grant, J., Soderblom, L., 2005. Water alteration of rocks and soils on Mars at the Spirit rover site in Gusev crater. Nature 436, 66–69.
Horgan, B.H.N., Anderson, R.B., Dromart, G., Amador, E.S., Rice, M.S., 2019. The mineral diversity of Jezero crater: evidence for possible lacustrine carbonates on Mars. Icarus 113526. https://doi.org/10.1016/j.icarus.2019.113526.
Kieffer, H.H., 2007. Cold jets in the Martian polar caps. J. Geophys. Res. Planets 112. https://doi.org/10.1029/2006JE002816.
Kim, S., Marrs, C., Nemer, M., Je-Hun Jang, J., 2017. Solubility model for ferrous iron hydroxide, hibbingite, siderite, and chukanovite in high saline solutions of sodium chloride, sodium sulfate, and sodium carbonate. ACS Earth Space Chem. 1, 647–663. https://doi.org/10.1021/acsearthspacechem.7b00065.
Kite, E.S., 2019. Geologic constraints on early Mars climate. Space Sci. Rev. 215, 10. https://doi.org/10.1007/s11214-018-0575-5.
Kounaves, S.P., Hecht, M.H., Kapit, J., Quinn, R.C., Catling, D.C., Clark, B.C., Ming, D.W., Gospodinova, K., Hredzak, P., McElhoney, K., Shusterman, J., 2010. Soluble sulfate in the martian soil at the Phoenix landing site: SULFATE AT THE PHOENIX LANDING SITE. Geophys. Res. Lett. 37, n/a-n/a. https://doi.org/10.1029/2010GL042613.
Lafuente, B., Downs, R.T., Yang, H., Stone, N., 2015. The power of databases: The RRUFF project. In: Highlights in Mineralogical Crystallography. De Gruyter, Inc., Berlin/München/Boston, GERMANY, pp. 1–30.
Leeman, W., 1982. Olivine Tholeiitic Basalts of the Snake River Plain, pp. 181–191.
Leeman, W., Vitaliano, C., 1976. Petrology of McKinney Basalt, Snake River Plain, Idaho. Geol. Soc. Am. Bull. 87, 1777–1792. https://doi.org/10.1130/0016-7606(1976)87<1777:POMBSR>2.0.CO;2.
Legett, C., Pritchett, B.N., Elwood Madden, A.S., Phillips-Lander, C.M., Elwood Madden, M.E., 2018. Jarosite dissolution rates in perchlorate brine. Icarus 301, 189–195. https://doi.org/10.1016/j.icarus.2017.06.031.
Leshin, L.A., Vicenzi, E., 2006. Aqueous processes recorded by Martian meteorites: analyzing Martian water on earth. Elements 2, 157–162. https://doi.org/10.2113/gselements.2.3.157.
Ling, Z., Wang, A., 2015. Spatial distributions of secondary minerals in the Martian meteorite MIL 03346,168 determined by Raman spectroscopic imaging. J. Geophys. Res. Planets 120, 1141–1159. https://doi.org/10.1002/2015JE004805.
Martínez, G.M., Renno, N.O., 2013. Water and brines on Mars: current evidence and implications for MSL. Space Sci. Rev. 175, 29–51. https://doi.org/10.1007/s11214-012-9956-3.
Martinez, I., Sanchez-Valle, C., Daniel, I., Reynard, B., 2004. High-pressure and high-temperature Raman spectroscopy of carbonate ions in aqueous solution. Chem. Geol. 207, 47–58. https://doi.org/10.1016/j.chemgeo.2004.02.003.
Martínez, G.M., Renno, N.O., Elliott, H.M., 2012. The evolution of the albedo of dark spots observed on Mars polar region. Icarus 221, 816–830. https://doi.org/10.1016/j.icarus.2012.09.008.
Martín-Torres, F.J., Zorzano, M.-P., Valentín-Serrano, P., Harri, A.-M., Genzer, M., Kemppinen, O., Rivera-Valentin, E.G., Jun, I., Wray, J., Bo Madsen, M., Goetz, W., McEwen, A.S., Hardgrove, C., Renno, N., Chevrier, V.F., Mischna, M., Navarro-González, R., Martínez-Frías, J., Conrad, P., McConnochie, T., Cockell, C., Berger, G. R., Vasavada, A., Sumner, D., Vaniman, D., 2015. Transient liquid water and water activity at Gale crater on Mars. Nat. Geosci. 8, 357–361. https://doi.org/10.1038/ngeo2412.
Mason, D.P., Elwood Madden, M.E., 2022. Raman spectroscopy of high salinity brines and ices. Icarus 372, 114759. https://doi.org/10.1016/j.icarus.2021.114759.
McEwen, A.S., Dundas, C.M., Mattson, S.S., Toigo, A.D., Ojha, L., Wray, J.J., Chojnacki, M., Byrne, S., Murchie, S.L., Thomas, N., 2014. Recurring slope lineae in equatorial regions of Mars. Nat. Geosci. 7, 53–58. https://doi.org/10.1038/ngeo2014.
McGraw, L.E., McCollom, N.D.S., Phillips-Lander, C.M., Elwood Madden, M.E., 2018. Measuring perchlorate and sulfate in planetary brines using Raman spectroscopy. ACS Earth Space Chem. 2, 1068–1074. https://doi.org/10.1021/acsearthspacechem.8b00082.
Moore, P.B., Ito, J., Steele, I.M., 1979. MacFallite and orientite: calcium manganese (III) silicates from upper Michigan. Mineral. Mag. 43, 325–331. https://doi.org/10.1180/minmag.1979.043.327.02.
Morales, J.W., Galleguillos, H.R., Hernández-Luis, F., Rodríguez-Raposo, R., 2011. Activity coefficients of NaClO4 in aqueous solution. J. Chem. Eng. Data 56, 3449–3453. https://doi.org/10.1021/je2005006.
Moyano-Cambero, C.E., Trigo-Rodríguez, J.M., Benito, M.I., Alonso-Azcárate, J., Lee, M. R., Mestres, N., Martínez-Jiménez, M., Martín-Torres, F.J., Fraxedas, J., 2017. Petrographic and geochemical evidence for multiphase formation of carbonates in the Martian orthopyroxenite Allan Hills 84001. Meteorit. Planet. Sci. 52, 1030–1047. https://doi.org/10.1111/maps.12851.
Nachon, M., Clegg, S.M., Mangold, N., Schröder, S., Kah, L.C., Dromart, G., Ollila, A., Johnson, J.R., Oehler, D.Z., Bridges, J.C., Mouélic, S.L., Forni, O., Wiens, R.C., Anderson, R.B., Blaney, D.L., Bell, J.F., Clark, B., Cousin, A., Dyar, M.D., Ehlmann, B., Fabre, C., Gasnault, O., Grotzinger, J., Lasue, J., Lewin, E., Léveillé, R., McLennan, S., Maurice, S., Meslin, P.-Y., Rapin, W., Rice, M., Squyres, S.W., Stack, K., Sumner, D.Y., Vaniman, D., Wellington, D., 2014. Calcium sulfate veins characterized by ChemCam/curiosity at Gale crater. Mars. J. Geophys. Res. Planets 119, 1991–2016. https://doi.org/10.1002/2013JE004588.
Nikolakakos, G., Whiteway, J.A., 2018. Laboratory study of adsorption and deliquescence on the surface of Mars. Icarus. Mars Polar Sci. VI 308, 221–229. https://doi.org/10.1016/j.icarus.2017.05.006.
Nuding, D.L., Rivera-Valentin, E.G., Davis, R.D., Gough, R.V., Chevrier, V.F., Tolbert, M. A., 2014. Deliquescence and efflorescence of calcium perchlorate: an investigation of stable aqueous solutions relevant to Mars. Icarus 243, 420–428. https://doi.org/10.1016/j.icarus.2014.08.036.
Ojha, L., Wilhelm, M.B., Murchie, S.L., McEwen, A.S., Wray, J.J., Hanley, J., Massé, M., Chojnacki, M., 2015. Spectral evidence for hydrated salts in recurring slope lineae on Mars. Nat. Geosci. 8, 829–832. https://doi.org/10.1038/ngeo2546.
Papadimitriou, S., Kennedy, H., Kattner, G., Dieckmann, G.S., Thomas, D.N., 2004. Experimental evidence for carbonate precipitation and CO2 degassing during sea ice formation. Geochim. Cosmochim. Acta 68, 1749–1761. https://doi.org/10.1016/j.gca.2003.07.004.
Phillips-Lander, C.M., Elwood Madden, A.S., Hausrath, E.M., Elwood Madden, M.E., 2019. Aqueous alteration of pyroxene in sulfate, chloride, and perchlorate brines: implications for post-Noachian aqueous alteration on Mars. Geochim. Cosmochim. Acta 257, 336–353. https://doi.org/10.1016/j.gca.2019.05.006.
Primm, K.M., Gough, R.V., Chevrier, V.F., Tolbert, M.A., 2017. Freezing of perchlorate and chloride brines under Mars-relevant conditions. Geochim. Cosmochim. Acta 212, 211–220. https://doi.org/10.1016/j.gca.2017.06.012.
Rennó, N.O., Bos, B.J., Catling, D., Clark, B.C., Drube, L., Fisher, D., Goetz, W., Hviid, S. F., Keller, H.U., Kok, J.F., Kounaves, S.P., Leer, K., Lemmon, M., Madsen, M.B., Markiewicz, W.J., Marshall, J., McKay, C., Mehta, M., Smith, M., Zorzano, M.P., Smith, P.H., Stoker, C., Young, S.M.M., 2009. Possible physical and thermodynamical evidence for liquid water at the Phoenix landing site. J. Geophys. Res. Planets 114. https://doi.org/10.1029/2009JE003362.
Rivera-Valentín, E.G., Chevrier, V.F., Soto, A., Martínez, G., 2020. Distribution and habitability of (meta)stable brines on present-day Mars. Nat. Astron. 4, 756–761. https://doi.org/10.1038/s41550-020-1080-9.
Rull, F., Maurice, S., Hutchinson, I., Moral, A., Perez, C., Diaz, C., Colombo, M., Belenguer, T., Lopez-Reyes, G., Sansano, A., Forni, O., Parot, Y., Striebig, N., Woodward, S., Howe, C., Tarcea, N., Rodriguez, P., Seoane, L., Santiago, A., Rodriguez-Prieto, J.A., Medina, J., Gallego, P., Canchal, R., Santamaría, P., Ramos, G., Vago, J.L., on behalf of the RLS Team, 2017. The Raman laser spectrometer for the ExoMars rover Mission to Mars. Astrobiology 17, 627–654. https://doi.org/10.1089/ast.2016.1567.
Rummel, J.D., Beaty, D.W., Jones, M.A., Bakermans, C., Barlow, N.G., Boston, P.J., Chevrier, V.F., Clark, B.C., de Vera, J.-P.P., Gough, R.V., Hallsworth, J.E., Head, J. W., Hipkin, V.J., Kieft, T.L., McEwen, A.S., Mellon, M.T., Mikucki, J.A., Nicholson, W.L., Omelon, C.R., Peterson, R., Roden, E.E., Sherwood Lollar, B., Tanaka, K.L., Viola, D., Wray, J.J., 2014. A new analysis of Mars "special regions": findings of the second MEPAG special regions science analysis group (SR-SAG2). Astrobiology 14, 887–968. https://doi.org/10.1089/ast.2014.1227.

Saheb, M., Neff, D., Bellot-Gurlet, L., Dillmann, P., 2011. Raman study of a deuterated iron hydroxycarbonate to assess long-term corrosion mechanisms in anoxic soils. J. Raman Spectrosc. 42, 1100–1108. https://doi.org/10.1002/jrs.2828.

Sass, Eytan, Ben-Yaakov, S., 1977. The carbonate system in hypersaline solutions: dead sea brines. Mar. Chem. 5, 183–199. https://doi.org/10.1016/0304-4203(77)90006-8.

Schon, S.C., Head, J.W., Fassett, C.I., 2012. An overfilled lacustrine system and progradational delta in Jezero crater, Mars: implications for Noachian climate. Planet. Space Sci. 67, 28–45. https://doi.org/10.1016/j.pss.2012.02.003.

Solomon, S.C., Aharonson, O., Aurnou, J.M., Banerdt, Wb, Carr, M.H., Dombard, A.J., Frey, H.V., Golombek, M.P., Hauck, S.A., Head, J.W., Jakosky, B.M., Johnson, C.L., McGovern, P.J., Neumann, G.A., Phillips, R.J., Smith, D.E., Zuber, M.T., 2005. New perspectives on ancient Mars. Sci. Wash. 307, 1214–1220. https://doi.org/10.1126/science.1101812.

Steiner, M.H., Hausrath, E.M., Elwood Madden, Megan, Tschauner, O., Elhmann, B.L., Olsen, A.A., Gainey, S.R., Smith, J.S., 2016. Dissolution of nontronite in chloride brines and implications for the aqueoushistory of Mars. Geochimica et Cosmochimica Acta. In press.

Temel, O., Karatekin, Ö., Mischna, M.A., Senel, C.B., Martínez, G., Gloesener, E., Van Hoolst, T., 2021. Strong seasonal and regional variations in the evaporation rate of liquid water on Mars. J. Geophys. Res. Planets 126, e2021JE006867. https://doi.org/10.1029/2021JE006867.

Tosca, N.J., McLennan, S.M., 2009. Experimental constraints on the evaporation of partially oxidized acid-sulfate waters at the martian surface. Geochim. Cosmochim. Acta 73, 1205–1222. https://doi.org/10.1016/j.gca.2008.11.015.

Vago, J.L., Westall, F., Coates, A.J., Jaumann, R., Korablev, O., Ciarletti, V., Mitrofanov, I., Josset, J.-L., De Sanctis, M.C., Bibring, J.-P., Rull, F., Goesmann, F., Steininger, H., Goetz, W., Brinckerhoff, W., Szopa, C., Raulin, F., Westall, F., Edwards, H.G.M., Whyte, L.G., Fairén, A.G., Bibring, J.-P., Bridges, J., Hauber, E., Ori, G.G., Werner, S., Loizeau, D., Kuzmin, R.O., Williams, R.M.E., Flahaut, J., Forget, F., Vago, J.L., Rodionov, D., Korablev, O., Svedhem, H., Sefton-Nash, E., Kminek, G., Lorenzoni, L., Joudrier, L., Mikhailov, V., Zashchirinskiy, A., Alexashkin, S., Calantropio, F., Merlo, A., Poulakis, P., Witasse, O., Bayle, O., Bayón, S., Meierhenrich, U., Carter, J., García-Ruiz, J.M., Baglioni, P., Haldemann, A., Ball, A.J., Debus, A., Lindner, R., Haessig, F., Monteiro, D., Trautner, R., Voland, C., Rebeyre, P., Goulty, D., Didot, F., Durrant, S., Zekri, E., Koschny, D., Toni, A., Visentin, G., Zwick, M., van Winnendael, M., Azkarate, M., Carreau, C., 2017. Habitability on early Mars and the search for biosignatures with the ExoMars rover. Astrobiology 17, 471–510. https://doi.org/10.1089/ast.2016.1533.

Vandenabeele, Peter, 2013. Practical Raman spectroscopy: an introduction / Peter Vandenabeele, Ghent University, Belgium., Analytical Techniques in the Sciences. Wiley, Chichester, West Sussex, United Kingdom.

Wang, A., Freeman, J.J., Jolliff, B.L., Chou, I.-M., 2006. Sulfates on Mars: a systematic Raman spectroscopic study of hydration states of magnesium sulfates. Geochim. Cosmochim. Acta 70, 6118–6135. https://doi.org/10.1016/j.gca.2006.05.022.

Wiens, R.C., Maurice, S., Perez, F.R., 2017. The SuperCam remote sensing instrument suite for the Mars 2020 rover: a preview. Spectrosc. Monmouth Junction 32, 50–55.